HIGHLY ACCURATE FREE SURFACE CAPTURING TECHNIQUE FOR WAVE BREAKING

Hidemi Mutsuda[1] and Yasuaki Doi[1]

We developed a new fluid solver that combines the advantages of both a Lagrangian scheme and an Eulerian scheme. The massless Lagrangian marker particles are put into the Eulerian grid and advected to capture accurately the free surface. The applicability of the present method was demonstrated for dam breaking, wave breaking in shallow water, impact pressure acting on a vertical wall. The efficiency and the accuracy were also investigated. The numerical results showed good agreement with numerical and experimental results performed by other researchers.

INTRODUCTION

This paper describes a new numerical model for the free surface evolution with wave breaking including a splashing and droplets using a coupled Eulerian-Lagrangian scheme. We developed a new fluid solver that combines advantages of both a Lagrangian scheme and an Eulerian scheme. A motivation for our work has been to describe wave deformation and air entrainment after breaking.

In existing numerical models, Volume of Fluid (Hirt et al., 1981), level set method (Sussman et al., 1994), CIP method (Yabe et al., 2001) and other Eulerian schemes are used as direct numerical simulation method for capturing free surface using a fixed Cartesian grid. On the other hand, SPH method (Gingold et al., 1977) and MPS method (Koshizuka et al., 1997) are a compressible and incompressible Lagrangian scheme whose flexibility and robustness allow to calculate complex free surface flows. Recently, to overcome various difficult problems demanding sophisticated methods for evolving free surface, Particle Level Set method (Enright et al., 2002), CLSVOF method and PLIC-VOF method have been presented. These methods provide impressible results. However, their numerical approach could be also costly and waste a lot of time on computing the smoothly evolving velocity field. Therefore, these methods cannot allow for higher spatial resolution and/or larger domain problem in order to achieve good performance and scalability.

In this paper, we propose a new fluid solver that combines advantages of both a Lagrangian scheme and an Eulerian scheme. Massless Lagrangian marker particles are put into the Eulerian grid and are advected according to velocity field in order to capture accurately free surface. In particle framework, the density function that describes free surface between different phases is corrected by using a suitable kernel function. The applicability of the present method is

[1] Hiroshima University, Graduate School of Engineering, Department of Social and Environmental Engineering, 1-4-1, Kagamiyama Higashi-Hiroshima, 739-8527, JAPAN

demonstrated for dam breaking, wave breaking in shallow water and impact pressure acting on a vertical wall. The efficiency and accuracy are also investigated.

NUMERICAL METHOD

In this section, the presented numerical techniques are described. The presented method employs the CIP method (Yabe et al., 2001) in a fixed Eulerian grid. In addition, to compute violent free surface motion with splashing and droplets accurately and efficiently, the method is coupled with Lagrangian marker particles. We call this the 'Particle CIP method'.

Governing Equations

The numerical model uses three or two dimensional incompressible Navier-Stokes equations. Conservation of mass and the density (color) function ϕ_I (gas: I =1 ; liquid: I =2 ; solid: I =3, respectively) is equation given by:

$$\frac{\partial u_i}{\partial x_i} = 0 \tag{1}$$

$$\frac{\partial u_i}{\partial t} + u_j \frac{\partial u_i}{\partial x_j} = -\frac{1}{\rho}\frac{\partial P}{\partial x_i} + \frac{\mu}{\rho}\frac{\partial^2 u_i}{\partial x_j \partial x_j} + F_e \tag{2}$$

$$\frac{\partial \phi_I}{\partial t} + u_j \frac{\partial \phi_I}{\partial x_j} = 0 \tag{3}$$

where $u_i = (u, v, w)$ is the velocity, μ the coefficient of viscosity in each phase, ρ the density in each phase, P the pressure, F_e the external force such as gravity acceleration and surface tension is modeled using the Continuum Surface Force (CSF) model proposed by Brackbill et al.(1992).

The density function ϕ_I ($0 \le \phi_i \le 1$) is used to define the physical properties of the different materials:

$$\phi_I = \begin{cases} 1 & \text{occupied} \\ 0 & \text{otherwise} \end{cases} \tag{4}$$

This density function can be used to track the interface between the substances of different density such as water, air and solids. The each phase is simulated with Navier-Stokes equations and variables such as viscosity, density and pressure may be discontinuous across the interface.

We can derive the density and the coefficient of the viscosity by using the density function on the grid:

$$\rho = \sum_{I=1}^{3} \rho_I \phi_I \tag{5}$$

$$\mu = \sum_{I=1}^{3} \mu_I \phi_I \tag{6}$$

where ϕ_I is the density function defined by (4).

Advection step and Non-advection step

The governing equations are solved using the fractional step method. It is well known that this technique is suitable for solving a multi-phase flow without smearing the density across the interface.

The advection step is calculated by the CIP method proposed by Yabe et al. (2001). The spatial profile of the density function between neighboring grids is approximated using a cubic interpolated function. The CIP method is a less diffusive and stable algorithm for solving the advection equation. We employ a Type-M scheme for the CIP method that is third-order accurate in time and space. In the CIP method, a spatial profile of a physical value between the cell faces of an Eulerian grid is interpolated by a cubic polynomial $F(x) = ax^3 + bx^2 + cx + d$ by using f and its derivative g in two grids. Then the spatial profile at $n+1$ step is obtained:

$$a_i = \frac{g_i + g_{iup}}{D^2} + \frac{2(f_i - f_{iup})}{D^3} \tag{7}$$

$$b_i = \frac{3(f_{iup} - f_i)}{D^2} - \frac{2g_i + g_{iup}}{D} \tag{8}$$

$$f_i^{n+1} = a_i X^3 + b_i X^2 + g_i^n X + f_i^n \tag{9}$$

$$g_i^{n+1} = 3a_i X^2 + 2b_i X + g_i^n \tag{10}$$

where $f^{n+1} = F(x - u\Delta t)$, $g^{n+1} = dF(x - u\Delta t)/dx$ and $X = -u\Delta t$. Here, $D = -\Delta x$, $iup = i - 1$ for $u \geq 0$ and $D = \Delta x$, $iup = i + 1$ for $u < 0$. In the Type M scheme, firstly, the CIP method is operated in one direction and then the first order scheme as a linear interpolation is operated in the other. The Type M scheme is sufficient for many applications. More details can be seen in Mutsuda et al.(2000).

The non-advection step is solved using the second-order finite difference method and we also solve a Poisson equation for the pressure with specified jump conditions:

$$\nabla\left(\frac{\nabla P^{n+1}}{\rho^*}\right)=\frac{\nabla\cdot u^*}{\Delta t} \tag{11}$$

where * denotes the physical value after the advection step. Both the pressure and its derivatives are clearly discontinuous between the different phases. Yabe et al. (2001) proposed the C-CUP method and applied this technique to multiphase flow without smearing the density, viscosity and pressure across the interface.

Arrangement of Grid and Particles

A staggered MAC grid arrangement is used to represent the velocity, density, coefficient of viscosity and pressure in a Cartesian computational grid as shown in Fig.1. The gray dots denote massless marker particles defined in the next section. The velocity components are defined on the cell faces of the grid. The pressure is defined at the center of the cell. The density function ϕ_I on the Eulerian grid is stored at the nodes of the grid. On the other hand, the density function ϕ_p is defined at the location of each massless marker particle. The value of the density function ϕ_p is kept constant during advection with the flow.

An explicit first order in time, fractional step method using the velocity projection method, is used to advance the velocity and pressure fields in time.

Lagrangian Marker Particles

To accurately and efficiently compute a violent free surface with splashing and droplets, we present a method based on the CIP method coupled with Lagrangian marker particles. These Lagrangian marker particles are passively advected with the flow and used not only to track the characteristics of the surface but also rebuild the density function in under-resolved regions where the bulk of the information is lost. To reduce computational cost, these particles are only located near the interface where the density function ϕ_I is discontinuous within a certain bandwidth. The diameter of all particles is half size of a grid unit and is also constant during a calculation. Four massless marker particles are set per grid in two dimensions and 8 in three dimensions.

Figure 2 shows one example of distribution of Lagrangian marker particles located in the inner region of a fluid. This example in our previous research is the numerical result of a strongly wave breaking on a reef in shallow water. The light blue area is the water region characterized by the density function $\phi_I = 1$. The black dots indicate Lagrangian marker particles set to sharply track the free surface. In this case, about 10,000 particles are located near the free surface.

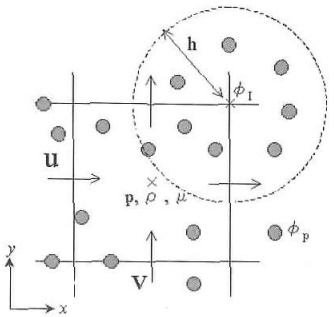

Figure 1. The arrangement of Grid and Particles

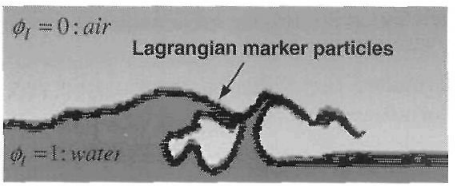

Figure 2. Example of particle distribution near the interface with the different densities (for a strongly wave breaking)

Time Integration of Particle Location

The particle locations are integrated using the evolution equation:

$$\frac{d\vec{x}_p}{dt} = \vec{u}(\vec{x}_p) \tag{12}$$

where $\vec{x}_p$ is the particle location and $\vec{u}(\vec{x}_p)$ is the particle velocity. The marker particles and the density function are separately integrated forward in time.

The equation for the particle locations is integrated using a forth order accurate Runge-Kutta method. The particle velocities $\vec{u}(\vec{x}_p)$ are interpolated from the velocities on the neighboring cell faces of the grid as mentioned in next section.

Particle Velocity $\vec{u}(\vec{x}_p)$ and Density Function ϕ_p

Particle velocities $\vec{u}(\vec{x}_p)$ are interpolated from their velocities against the underling grid, and the density function ϕ_p defined for the particles is interpolated from the density function ϕ_I defined on the nodes of the grid. In the presented method, we use bilinear or trilinear interpolation depending on the required accuracy and efficiency. Since the velocities on the cell faces are exchanged in unsteady flow problems, the procedure of the interpolation is performed at each time step.

Error Correction of Density Function ϕ_I

We propose a method for reconstructing an interface using Lagrangian marker particles. The error of the density function ϕ_I defined on nodes of the grid is corrected by using the neighboring particles within the interaction region with a radius h as shown in Fig.1. A smooth approximation of the density function ϕ_I can be constructed using a kernel function in the SPH method (Gingold et al., 1977). This approximation is popular as particle methods.

In the presented method, as we use the SPH method with a kernel function, the density function ϕ_I defined on nodes of the grid is corrected using the density function ϕ_p defined at the Lagrangian marker particles within the referenced area with radius h:

$$\phi_I' = \max\left(\phi_I, \sum_{j=1}^{N} \phi_p \frac{m_p}{\rho_p} W_p\left(\left|x_g - x_p\right|, h\right) \right) \tag{13}$$

where ϕ_I' is the density function on nodes of the grid after collecting the error, m_p / ρ_p is the volume characterized by the radius r_p of the particle, W_p is the kernel function defined as a spline function and x_g and x_p indicate spatial variables on a grid and a particle, respectively. The referenced radius h is set to twice the grid size. This procedure for error correction of the density function is carried out periodically. It is not necessary to perform this procedure at each time step.

Redistribution of Particles

To accurately capture the interface during a calculation, the redistribution process of the Lagrangian marker particles near the discontinuous interface is required. Particles are added and deleted in the grid near the interface using a level set function ψ ($-\infty < \psi < +\infty$, $\psi = 0$ at the interface) constructed by the density function ϕ_I. It is noted that the level set function defined in the present method is not advected to track the interface as the Level Set Method does that, rather, it is only used to build a level set contour at a certain time.

The interface between two phases is found by the density function ϕ_I defined on nodes of the grid. The gradient $\partial\phi_I / \partial x_i$ of the density function ϕ_I in space obtains a maximum value near the interface. Therefore, we can estimate the interface at a point in time using the following conditions for the x-direction:

$$\left\{ 1 + \alpha \left(\frac{\partial \phi_I}{\partial x} \right)^2 \right\}^{\frac{1}{2}} \geq \frac{f_{crt}}{\min(dx, dy, dz)} \tag{14}$$

where f_{crt}, a parameter that is dependent of grid size, is set to 0.1 to work well here and α is set to twice the grid size. Using the same approach, the interface for the y- and z-directions, can be easily estimated. Using these conditions, the level set function $\psi(x,y,z)$ is set to zero at the interface and the level set contour is constructed in a calculation domain.

After constructing the level set contour, Lagrangian marker particles are redistributed in the inner region where the distance from the interface is within a bandwidth α, and the density function ϕ_l is greater than 0.5, for example the liquid phase.

After the redistribution process, the located Lagrangian particles are attracted to the current smooth interface characterized by the level set function $\psi = 0$. The previous location $x_{p,old}$ of the particle before attraction is replaced using eq.(15) proposed by Enright et al.(2002) :

$$\vec{x}_{p.new} = \vec{x}_{p,old} + \lambda(\psi_{goal} - \psi(\vec{x}_p))\vec{N}(\vec{x}_p) \tag{15}$$

where $x_{p,new}$ is the new location of the particles, λ =1. $\psi(\vec{x}_p)$ is the level set function at the location, x_p, of each particle and is obtained by the interpolation as mentioned in previous section. $\vec{N}(\vec{x}_p)$ and ψ_{goal} are defined in Enright et al.(2002). To capture a more sophisticated interface, after the redistribution process, we put one particle per grid at the location where the following condition is satisfied.

$$\alpha < \psi(x,y,z) < \gamma \tag{16}$$

where γ is dependent on a flow condition and set to 4 to 6 times the grid size in this paper. We select α =2.0 to work well in the present method. Finally, a particle is deleted from a computational domain when $\psi(\vec{x}_p) < 0$. The procedure for particle redistribution is only carried out when the volume error of the liquid phase exceeds a limit condition not at each time step.

RESULTS AND DISCUSSIONS

Collapsing of Water Column

The water column is H =1.2m wide and h =0.6m high. The calculation domain is 3.22m wide and 1.2m high. The water column is initially set on the left side with a rectangular shape. A 214×80 grid domain is used in two dimensions. The grid size is 15mm. The density and coefficient of viscosity are 1,000kgm^{-3} and 1.0×10^{-3} Pa.s in the water region, and 1.25kgm^{-3} and 1.82×10^{-5}Pa.s in the air region, respectively. The total number of the particles near the free surface is

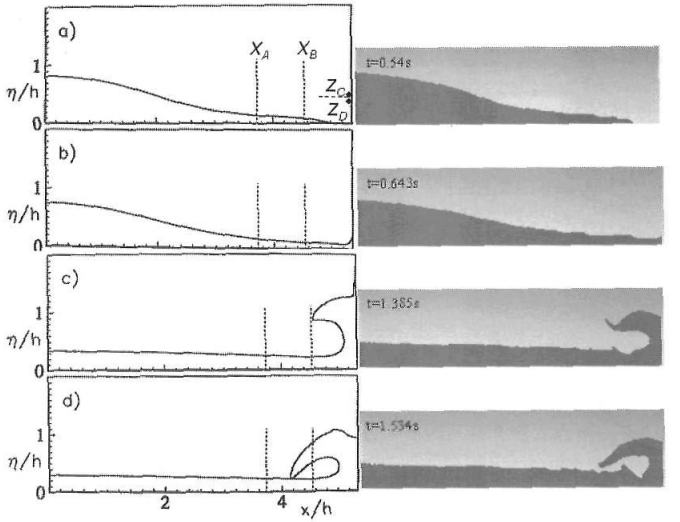

Figure 3. Comparison of the free surface deformation after the collapsing of the water column (Left : BEM results by Greco et al., 2001, Right : Present results)

1,509 in two dimensions. The increment of the initial located particles is 7.5mm. The free-slip condition is imposed on all boundaries. The time increment is 10^{-4} s and the calculation time is 5s.

Figure 3 shows a comparison of the free surface deformation with BEM results (Greco et al., 2001). Our numerical results are in overall agreement with Greco's numerical results. Next, water elevations are compared at both $X_A/h = 3.721$ and $X_B/h = 4.542$ where the water is overturning and touching down after colliding with the right wall as shown in Fig.3.

The pressure is also compared at both $Z_C/h = 0.27$ and $Z_D/h = 0.19$. Figure 4 shows a comparison over time of the water elevations at the locations X_A and X_B . The model is in good agreement with the experimental and numerical results (Greco et al., 2001 ; Zhou et al., 1999) at t=1.534s when the water is touching down. After touching down, the splashed water causes a complicated flow containing air bubbles; here, the model is not in such good agreement with the experimental results. However, the tendency of the time sequence is quite good at both positions.

Figure 5 shows comparison over time of the pressure at both $Z_C/h = 0.27$ and $Z_D/h = 0.19$ on the right wall. The presented model is in quite good agreement with the experimental and numerical results during the calculation time, especially from t=1.5s to 2.0s when the water is colliding with the right

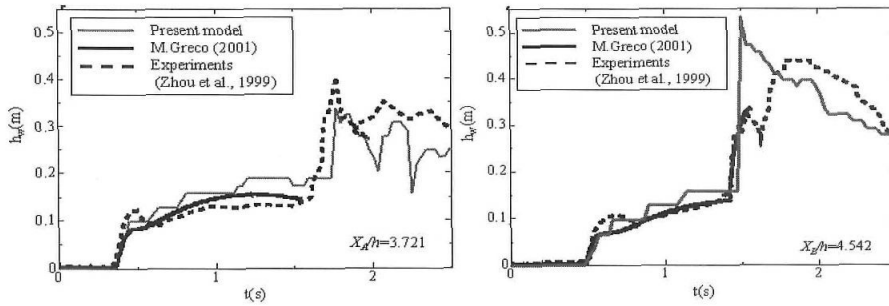

(a) X_A/h=3.721 (b) X_B/h=4.542

Figure 4. Comparison of the water elevations at X_A and X_B near the right wall

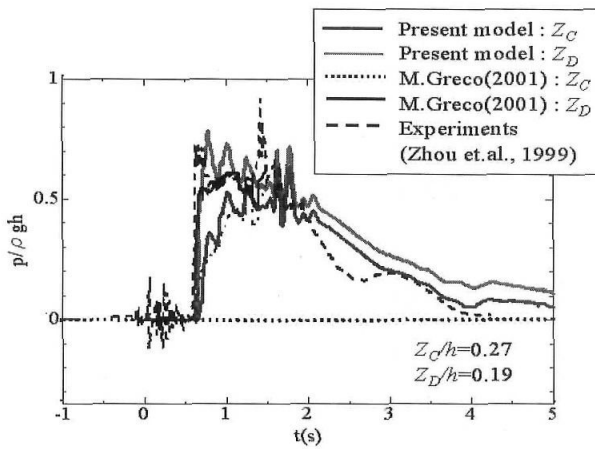

Figure 5. Comparison of the time history of the pressure at Z_C and Z_D on the right wall

wall. The time line for oscillating and decreasing has the same tendency, and the peak pressure coincides with the other results.

Wave Breaking on a Reef

Figure 6 shows a large scale wave breaking process over a reef without a vertical wall. It can be seen that the present method can calculate the droplets, the fluid pouring and the splashing after the strongly wave breaking in comparison with other numerical method. The grid size is 2.68mm in x-direction and 3.89mm in y-direction and the increment between particles is 1.34mm. The

grid number is 248×57 in 2D. The time increment is 10^{-4}s. About 4,700 particles are located near the free surface at the initial condition to capture the free surface. The incident wave height H is H/h =0.473, where h is the initial water depth.

Figure 7 shows the time history of the volume error in the water region in this case. The volume error means the ratio of the water volume to the initial state. The error is limited to less than $\pm 0.05\%$ throughout the calculation and the average is about $\pm 0.02\%$. It is noted that the volume error in the water region is corrected at regular time intervals using the Lagrangian marker particles near the free surface.

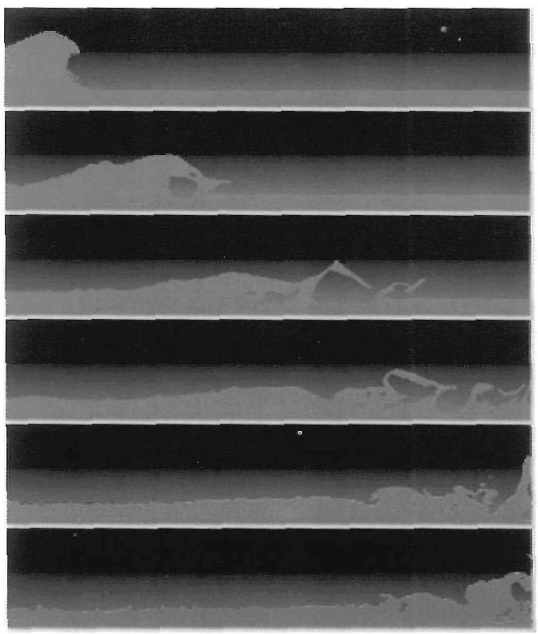

Figure 6. Wave breaking process on a reef (Breaker type : Plunging Breaker)

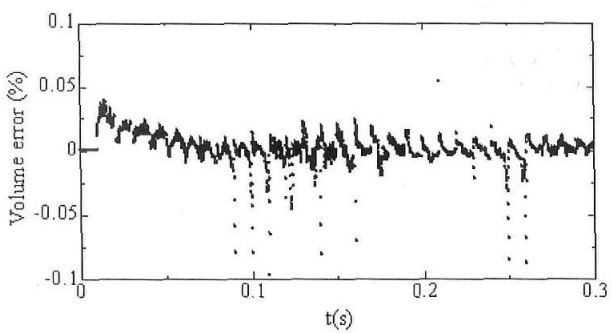

Figure 7. Time variation of volume error in water region.

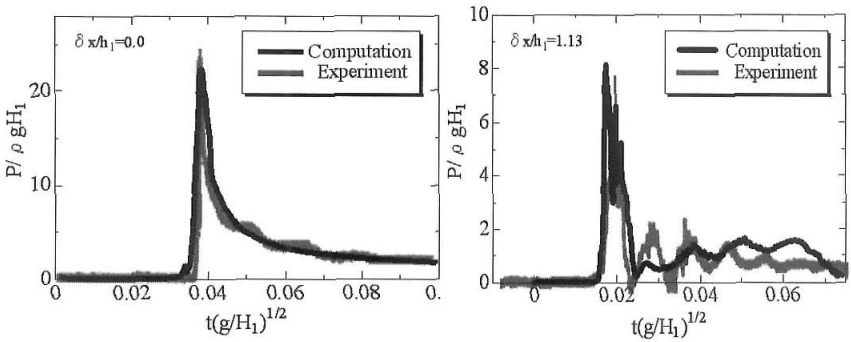

(a) Wagner type (b) Bagnold type

Figure 8. Time history of impact pressure without entrained air.

Figure 8 shows a comparison of the time variation of pressure for both Wagner and Bagnold types. Black lines denote the experimental results (Ararmsa et al., 1996), and blue and red lines are our results. Z/h_1 is the non-dimensional vertical position from the still water level. Our numerical results are in good agreement with the experimental results, especially for the Wagner type pressure, as seen in Fig. 8 (a). As shown in Fig. 8(b), for the Bagnold type pressure, our numerical results are in good agreement with the experimental results. The frequency of oscillation ranges from 20 to 100Hz in our numerical results. However, in the experimental results, it is higher frequency, 160Hz. It is seen that both the frequency of oscillation and the amount of trapped air are correlated to the dynamics of the entrained air during the impact.

Figure 9 shows a comparison of the vertical distribution of maximum pressure at several vertical locations, Z/h_1 =-0.052～1.349 on the wall located at three horizontal positions: δ_x/h_1 =-0.53 (before breaking point), δ_x/h_1 =0.47 (near breaking point) and δ_x/h_1 =1.13 (after breaking point). Blue lines denote the present method, Red triangles denote our previous work without Lagrangian particles, and open circles are the experimental results with deviations. The maximum pressure is in overall agreement with the experimental results at all locations, except for pressure values at $Z/h_1 \approx 0.6$ (δ_x/h_1 =0.47) and $Z/h_1 \approx 0.3$ (δ_x/h_1 =1.13), although the fluctuations in the maximum pressure are observed in the experimental results.

CONCLUSIONS

To investigate applications in coastal and ocean engineering, we have developed an interface capturing method with the Lagrangian marker particles

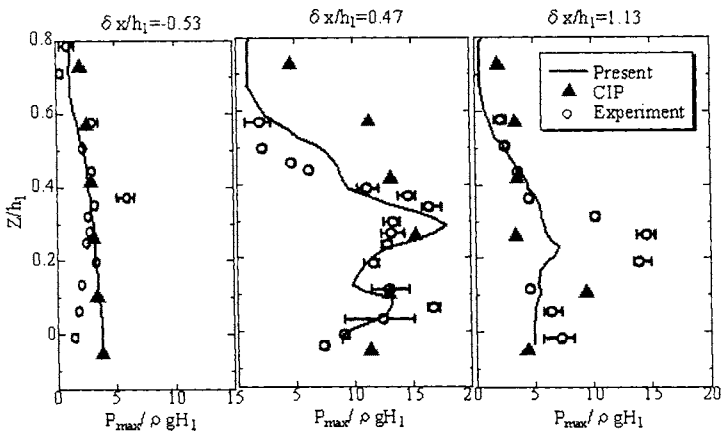

Figure 9. Comparison of vertical distribution of maximum impact pressure on a vertical wall at three different locations.

and named this the 'Particle CIP' method. The present method was applied to wave breaking with air entrainment in shallow water and impact pressure acting on a wall in Wagner type and Bagnold type.

Comparing with previous numerical and experimental results, our numerical results were in good agreement. The presented method is capable of computing flows involving both air and water phases. It can accurately simulate wave breaking and splashing with air entrainment, and is very robust for violent wave phenomena in both two and three dimensions. The impact pressure due to Wagner and Bagnold types was also compared with experimental results and can be directly estimated using the presented method.

The present numerical method should be a useful tool for a wide range of coastal and ocean engineering. In future work, the present method will be combined with the SPH method to compute interaction between wave and an elastic structure. We will investigate the fluid-structure interaction with hydro-elastic response due to wave impact.

ACKNOWLEDGMENTS

The present study activity was supported by the Center for Ships and Ocean Structure, NTNU, and the research was partly performed in staying at Stanford University.

REFERENCES

Azarmsa S. Ali. 1996. Impact pressure and decay properties of breaking waves, *Dr thesis, Gifu University*, 96p

Brackbill, J. U., Kothe, D.B. and Zemach, C. 1992. Acontinuum method for modeling surface tension, *J. Comput. Phys.*, 100, 335-354.

Enright, D., R. Fedkiw, J. Ferziger and I. Mitchell. 2002. A hybrid particle level set method for improved interface capturing, *J. Comput. Phys.*, Vol.183, No.1, 83-116.

Gingold R.A., J. J. Monaghan. 1977. Smoothed particle hydrodynamics, theory and application to non-spherical stars, *Mon. Not. Roy. Astr. Soc.*, Vol.181, 375-389.

Greco M. 2001. A two-fimensional study of Green-Water Loading, *PhD. thesis*, Norwegian University of Science and Technology, 150p.

Hirt, C.W. and B.D.Nichols. 1981. Volume of fluid (VOF) method for the dynamics of free boundaries, *J. Comput. Phys.*, 39, 201-225.

Koshizuka, S. and Oka, Y. 1996. Moving-Particle Semi-implicit Method for Fragmentation of Incompressible Fluid, *Nul. Sci. Eng.*, 123, 421-434.

Mutsuda, H. and T.Yasuda. 2000. Numerical Simulation of turbulent air-water mixing layer within surf-zone, *Proc. 27th Int. Conf. on Coastal Eng.*, 755-768.

Sussman M., Smereka P. & Osher S. 1994. A Level Set Approach for Computing Solutions to Incompressible Two-Phase Flow, *J. Comput. Phys.*, 114, 146-159.

Yabe, T., Xiao, F., Utsumi, T. 2001. Constrained interpolation profiles method for multiphase analysis, *Journal Computational Physics*, Vol.169, 556-593.

Zhou, Z. Q., Katm J. Q. D. and Buchner, B. 1999. A nonlinear 3-d approach to simulate green water dynamics on deck. In Piquet (Ed.), *Proc. 7th Int. Conf. Num. Ship Hydrod.*, Natures, France, 5.1-1, 15.